Ionic liquid-assisted synthesis of Yb^{3+}-Tm^{3+} Codoped $Y_7O_6F_9$ Petal Shaped Microcrystals with enhanced upconversion emission

Jinbo Zhao,[a*] Lili Wu,[b,c,*] Chuanjiang Zhang,[a] Tingxi Li,[d,]

Qinglong Jiang,[e] Feng Wang,[a] Ping Zhao,[a] Jong Eun Ryu,[f] and Zhanhu Guo [c,*]

[a] School of Materials Science and Engineering,
Qilu University of Technology (Shandong Academy of Sciences),
Jinan, 250353, China.

[b] School of Materials Science and Engineering,
Shandong University,
Jinan, 250061, China.

[c] Integrated Composites Laboratory (ICL),
Department of Chemical and Biomolecular Engineering,
University of Tennessee, Knoxville, TN 37996 USA

[d] College of Materials Science and Engineering, Shandong University of Science and Technology,
Qingdao 266590, China

[e] Materials Science Division,
Argonne National Laboratory, Lemont, IL 60439, USA

[f] Department of Mechanical Engineering,
Indiana University-Purdue University Indianapolis,
Indianapolis, IN 46202, USA

* to whom the correspondence should be addressed

Email: zjbwll@163.com (J. Zhao), wulili@sdu.edu.cn (L. Wu) and zguo10@utk.edu (Z. Guo)

This is the author's manuscript of the article published in final edited form as:

Zhao, J., Wu, L., Zhang, C., Li, T., Jiang, Q., Wang, F., … Guo, Z. (2018). Ionic liquid-assisted synthesis of Yb3+-Tm3+ codoped Y7O6F9 petal shaped microcrystals with enhanced upconversion emission. Materials Research Bulletin, 103, 19–24. https://doi.org/10.1016/j.materresbull.2018.03.003

Graphical abstract

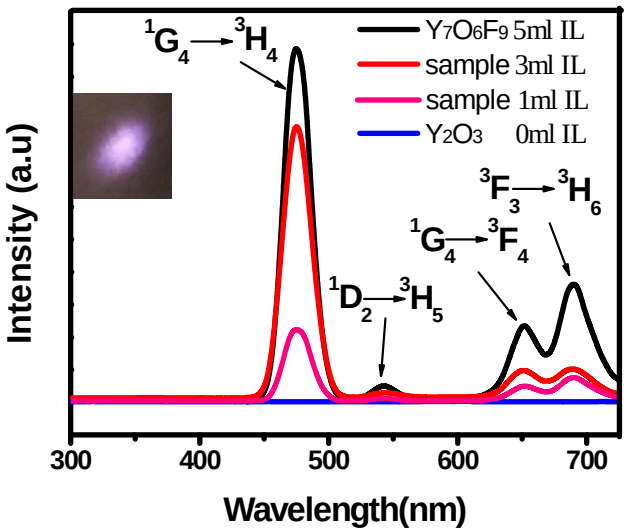

Petal-like Yb^{3+}-Tm^{3+} codoped $Y_7O_6F_9$ microparticles were achieved via ionic liquid-assisted hydrothermal process. Bright visible luminescence can be seen clearly with 980nm laser diode excitation power as low as ~ 0.1W/cm^2 (pump power 10 mW).

Hightlights

- Petal-like Yb^{3+}-Tm^{3+} codoped $Y_7O_6F_9$ microparticles were achieved via fluorinated ionic liquids assisted-hydrothermal process
- Enhanced bright luminescence can be seen clearly with 980nm laser diode at low excitation power (pump power 10 mW).

Abstract

Petal-like Yb^{3+}-Tm^{3+} codoped $Y_7O_6F_9$ microparticles were achieved via ionic liquid-assisted (IL) hydrothermal process. The emission efficiency of $Y_7O_6F_9$: Yb^{3+}/Tm^{3+} powders is much stronger than that of Y_2O_3: Yb^{3+}/Tm^{3+} sample. Under excitation at 980 nm with an unfocused laser beam

under weak pump density of ~0.1 W/cm^2 (pump power 10 mW), the UC emission of the sample can been seen clearly. Four emission bands at 477, 540, 647 and 692 nm are observed and correspond to the $^1G_4$ state to $^3H_6$ state, $^1D_2$ state to $^3H_5$ state, $^1G_4$ sate to $^3F_4$ state, and $^3F_3$ state to $^3H_6$ state transition of Tm^{3+} ions. The enhanced UC emission is related to high crystallinity and lower effective phonon energy of oxyfluorides. The ionic liquid (IL) of [BMIM][BF_4] is used both as the reaction medium and the source of F^-.

Keywords: Up-conversion photoluminescence; $Y_7O_6F_9$: Yb^{3+}/Tm^{3+}; 980 nm excitation; Ionic liquid; Optical materials and properties.

1. Introduction

Upconversion crystals can convert two or more near-infrared (NIR) photons to one high energy photon in the ultraviolet (UV) or visible regions [1-2], which are useful for various potential technological applications such as solid-state laser, efficient solar cells, display, bioimaging and biomedicine [3-7]. Among various UC materials, the synthesis and design of lanthanide-doped microstructure is one major focus [8-13], due to the ladder-like 4f energy levels which have more than one intermediate long-lived level and can principally be used to produce UC luminescence [8]. Fluorides are reported to be efficient host materials for the UC crystals due to their low effective phonon energy [14-16]. However, due to the thermal instability and air sensitivity, it is not suitable for fluorides based crystals to be used as host materials, which greatly limit their applications. For numerous applications, the lower upconversion efficiency is still a bottleneck

problem. Thereby, it is critical to explore new host materials for enhancing upconversion efficiency.

With unique physical, chemical and optical properties, such as high thermal stability and low phonon cutoff energy, Y_2O_3 would be an outstanding candidate for rare-earth doped host material[17-19]. But the higher phonon energy for the oxides than that of fluorides decreases the UC efficiency. Oxyfluorides, combining the advantages of both fluoride and oxide crystals, not only have better chemical and thermal stability than fluorides but also have effective lower phonon energy than oxides [20]. Recently, a number of oxyfluorides compounds have been prepared and studied, such as YOF: Er^{3+}, Yb^{3+}; GdOF: Er^{3+}, Yb^{3+}; LaOF: Er^{3+}, Yb^{3+}; $Y_6O_5F_8$: Er^{3+}, Yb^{3+}; $Y_7O_6F_9$: Eu^{2+}, Mn^{2+} and $Y_7O_6F_9$: Yb^{3+}, Tm^{3+} [21-25]. Among these works, the $Y_7O_6F_9$ powders codoped with Yb^{3+} and Tm^{3+} ions was first successfully achieved by co-precipitation and subsequent calcining route. The hydrofluoride acid was used as the source of F^-. The samples showed intense ultraviolet and blue upconversion emissions under 980 nm laser excitation in their works [20]. However, the excitation power density of 1 W/cm^2 is still high.

In this paper, enhanced upconversion photoluminescence of $Y_7O_6F_9$:Yb^{3+}/Tm^{3+} microcrystals is reported under excitation of 980 nm with low excitation power density. 980 nm wavelength well matches the absorption of Yb^{3+} [26], providing an ideal excitation source for UC emission. Bright visible luminescence was observed to the naked eye clearly under excitation power of ~0.1 W/cm^2, (pump power 10 mW). The mechanism for the enhanced UC emission attributes to the well crystalline structures and the lower phonon energy of oxyfluorides.

2. Experimental

2.1 Materials

All the reagents were of analytical grade and were used as received without further

purification. Yttrium nitrate hexahydrate ($Y(NO_3)_3 \cdot 6H_2O$), thulium nitrate hexahydrate ($Tm(NO_3)_3 \cdot 6H_2O$) and ytterbium trinitrate pentahydrate ($Yb(NO_3)_3 \cdot 5H_2O$) were obtained from Aladdin Reagent Co. Ltd. Hexamethylenetetramine (HMT, $C_6H_{12}N_4$, Mw = 140.19) were obtained from Sinopharm Chemical Reagent Shanghai Co. Ltd. Deionized water was used to prepare the solutions. N-methylimidazole, n-butyl bromide, potassium tetrafluoroborate (Aladdin Reagent Co. Ltd.) and ethyl ether were used to prepare [BMIM][BF_4] ionic liquid (IL). The synthesis procedure of [BMIM][BF_4] is designed just as reported [27]. Briefly, N-methylimidazole and n-butyl bromide were mixed and then the mixture was irradiated in the household microwave oven (Haier) for 30 s at 240 W. The reaction mixture was taken out, standing for 30 s, and then heated at the same power level for 15 s. This step is repeated 8 times. The unreacted starting materials were removed by washing with ethyl ether. After that, excess potassium tetrafluoroborate was added into the prepared solution and then irradiated in the microwave oven for 10 s at low power again. This step repeated 6 times. After getting rid of the precipitation, the [BMIM][BF_4] was prepared.

2.2 Synthesis of Yb^{3+}/Tm^{3+} Co-doped nanocrystals of $Y_7O_6F_9$

In a typical experiment, 0.5827 g yttrium nitrate hexahydrate, 0.0764 g ytterbium trinitrate pentahydrate, 0.0039 g thulium nitrate hexahydrate and 0.357 g HMT were dissolved in 12 mL deionized (DI) water, and then 5 mL ionic liquid of [BMIM][BF_4] was added in the solution. After vigorous stirring for 1 h at room temperature, the final solution was put into a sealed 20 mL teflon-lined stainless autoclave, and heated at 180 °C for 24 hours in an oven. The obtained precipitates were collected by centrifugation, rinsed by deionized water and ethanol for several times and then dried in air at 60 °C for 24 h. After calcined at 700 °C for 4 h, the powders were collected for further characterizations. Keeping the other conditions the same, samples with different concentrations of IL were prepared to investigate the influence of [BMIM][BF_4] on the

morphologies and properties of products. In addition, without adding IL, the sample Y_2O_3: Yb^{3+}, Tm^{3+} microspheres with the same doping condition was also prepared by the same method. In order to investigate the influence of doping concentration of Tm^{3+} on the luminescence properties, the $Y_7O_6F_9$ (5 mL IL) microcrystals at different doping concentration (Yb: Tm=10:*x* mol%, *x*= 0.1, 0.3, 0.7) were synthesized, keeping other experiment conditions as same as before.

2.3 Characterizations

X-ray diffraction (XRD) measurements were performed for the prepared powders by using a Rigaku Dmax2200 X-ray diffractometer with Cu Ka radiation (λ = 1.5406 Å) at 40 kV and 150 mA. The morphologies of the samples were observed by the field-emission scanning electron microscope (FE-SEM Hitachi S-4800, 5 kV). UC luminescence spectra of the samples were recorded by a spectrophotometer (970CRT, Shanghai Precision Instrument Factory, China) with a 980 nm optical fiber laser (DS3-11312, BWT, Beijing Kaipulin Co., LTD, China) as the excitation source. Raman spectra were obtained on Renishaw InVia Reflex.

3. Results and discussion

3.1. Crystal Structure

Fig. 1 shows XRD patterns of the prepared calcinated samples. For the sample without IL, broader diffraction peaks can be observed. The diffraction peaks are in good agreement with the standard values for Y_2O_3 (JCPDS file No. 82-2415). With the IL added to 1 mL, phase transition occurs and diffraction peaks of $Y_7O_6F_9$ were observed. It means F^- in IL replaced the O^{2-}, but it is not enough to replace all O^{2-}. This result is similar with the work of Park et al. [26]. When 3 mL IL was used in the solution, all the XRD diffraction peaks can be indexed as $Y_7O_6F_9$ (JCPDS 80-1126). With further increasing the IL to 5 mL, the $Y_7O_6F_9$ diffraction peaks become sharper,

implying that the crystallinity of the sample is good and the grain size of the sample is growing up. The $Y_7O_6F_9$ sample was achieved just by adjusting the dosage of IL. No peaks of any other phase are detected. And the co-doping of Yb^{3+} and Tm^{3+} ions does not influence the crystal structure too. In addition, with the increase of IL concentration, the XRD diffraction peaks become sharper and the crystallinity of the sample become better. The good crystallinity will be beneficial to the UC photoluminescence of the materials.

Fig. 2 presents the FE-SEM images of the samples after calcination. It shows that the structure of the $Y_7O_6F_9$:Yb^{3+}/Tm^{3+} (with 5 ml IL) is petal shaped microsphere with uniform size and good dispersity. The mean diameter of the microsphere is 2.5 μm, Fig. 2a. It can be seen that the small particles are the building blocks for the petal shaped microspheres (Fig. 2b). In order to understand the formation process of the microspheres, the effect of concentration of IL on the morphology of products was also investigated. In this case, it was found that the concentration of IL was key factor to influence the morphology of the products. Fig. 2c and Fig. 2d show the Y_2O_3:Yb^{3+}/Tm^{3+}microspheres synthesized without IL. In Fig. 2d, we can see that the microspheres are consisted of nano-plates with 50 nm in thickness. In the hydrothermal process, when 16 mL DI water and 1 mL [BMIM][BF_4] were used as the medium, well dispersed nanoparticles were obtained and the nanoparticles look like many scattered petals (Fig. 2e). Fig. 2f shows the sample prepared in 3 mL [BMIM][BF_4] and 14 mL deionized water. In the sample, the basic self-organization structures of the petal have been formed, and there are still many scraps that can be seen. Increasing the IL concentration (when 5ml [BMIM][BF_4] and 12 mL deionized water were used), the $Y_7O_6F_9$:Yb^{3+}/Tm^{3+} microcrystals were synthesized and the morphology of sample changed from simple nanoparticles to petal shaped microspheres (Fig. 2a). The grain size of $Y_7O_6F_9$: Yb^{3+}/Tm^{3+} is growing up to 2.5 μm.

In the experiments, the IL of [BMIM][BF_4] not only participates the reaction as the source of F^- but also plays as a growth template in controlling the morphology of the products. The IL has lower interfacial tension as well as higher viscosity than water. The lower interfacial tension of the medium can let more nuclei produced in the nucleation process, but the effective diffusion of the nuclei was lowered when the viscosity was higher in the medium. Then, the newly produced nuclei will be inclined to attach on the surface of larger crystals which led to the self- assembled petal shaped microstructure (Fig. 2a) [29,30]. This diffusion-limited growth model is also mentioned in our previous work [29].

3.2. UC Emissions

The UC emissions spectra of the samples were studied in the visible and ultraviolet wavelength from 300-725nm. Fig. 3a shows the UC spectra of the samples under a weak unfocused excitation at 980 nm of ~0.1 W/cm^2 (pump power 10 mW) and bright luminescence was visible to the naked eye. The $Y_7O_6F_9$:Yb^{3+}/Tm^{3+}powders have multicolor UC emission, Fig.3a. The emission efficiency of $Y_7O_6F_9$: Yb^{3+}/Tm^{3+} is much stronger than that of Y_2O_3: Yb^{3+}/Tm^{3+} sample. In the UC emission spectra (Fig. 3a), there are four emission bands at 477, 540, 647, and 692 nm, which correspond to the $^1G_4$ state to $^3H_6$ state, $^1D_2$ state to $^3H_5$ state, $^1G_4$ state to $^3F_4$ state, and $^3F_3$ state to $^3H_6$ state transition of Tm^{3+} ions, respectively [31]. Fig.3a shows the effect of the IL concentration on the upconversion emission spectrum. The UC emission intensity enhanced remarkably with increasing IL concentration, which is consistent with the XRD results that the Y_2O_3 phase was transformed into $Y_7O_6F_9$ phase with the increase of IL concentration. As shown in the inset of Fig. 3a, the bright UC luminescence in $Y_7O_6F_9$:Yb^{3+}/Tm^{3+} (5 mL IL) microsphere can be easily observed by our naked eyes even at laser pump power density of only ~0.1 W/cm^2 (pump power

10 mW). In a further set of experiments, the influences of concentration of doping ions Tm^{3+} were explored. Compare to $Y_7O_6F_9$:Yb^{3+}/Tm^{3+}, the UC emission intensity of Y_2O_3: Yb^{3+}/Tm^{3+} was not observed at the same pump power (10 mW), Fig. 3a. Until the pump power was increased to 1000 mW, the Y_2O_3: Yb^{3+}/Tm^{3+} powders produce UC emissions (Fig. 3b). The emission bands locate at 477, 540, 647, and 692 nm, which is the same as the $Y_7O_6F_9$:Yb^{3+}/Tm^{3+} sample. The upconversion emission spectra of $Y_7O_6F_9$ (5 mL IL) at different doping concentration (Yb: Tm=10:*x* mol%, *x*= 0.1, 0.3, 0.5. 0.7) are shown in Fig. 3c. It is clearly seen from Fig. 3c that different doping concentrations of Tm^{3+} ions lead to differences of relative intensities of each emission position. With increasing the Tm^{3+} ion content from 0.1 to 0.5%, the emission intensities increase. Due to the occurrence of Tm^{3+} ion concentration quenching [32], the intensities begin to fall when the concentration of Tm^{3+} ion reaches 0.7%.

The enhanced upconversion for the $Y_7O_6F_9$: Yb^{3+}/Tm^{3+} microspheres under 980 nm excitation can attribute to high crystalline structures and low phonon energy. The high crystalline structures are due to the use of IL solution. Increase the dosage of IL, crystallinity of the samples increased and the intensity of UC photoluminescence also increased. The well-crystallized structures of the microspheres exert a strong crystal field around the dopant ions and minimize the energy loss of the dopant ion arising from crystal defects [33]. Then the enhanced upconversion of the $Y_7O_6F_9$: Yb^{3+}/Tm^{3+} microspheres was achieved. Host materials with low phonon energy may decrease the probability of nonradiative transitions, subsequently leading to high luminescence efficiency [8]. The phonon energies of the samples were characterized by Raman spectra (Fig.4). The Stokes Raman shifts of $Y_7O_6F_9$ and Y_2O_3 are measured at the same condition at room temperature. Under the excitation of 532 nm, Fig.4 shows the Raman shifts peaks of the samples in the range of 100-1000cm^{-1}. The Raman peaks at 364, 431, 498, 717 and 761cm^{-1} are

the Raman shifts of $Y_7O_6F_9$ sample (Fig. 4 a). And the maximum phonon vibration of $Y_7O_6F_9$ can be found at 364 cm^{-1}. The peaks at 208, 241, 376, 472, 504, 552, 588, 636, 724, 809 and 962 cm^{-1} are the Raman shifts of Y_2O_3 sample (Fig. 4 b). For Y_2O_3 sample, the maximum phonon vibration is at 472 cm^{-1}. The effective phonons energy can be shown as $\hbar\omega_m$ where ω_m is assumed to be the maximum lattice frequency [14]. The effective phonons energy can be used to estimate the comparative emission intensity of the samples. $Y_7O_6F_9$ which have the low effective phonon energy show high efficiency UC luminescence than Y_2O_3 microspheres. The upconversion efficiency of the $Y_7O_6F_9$: Yb^{3+}/Tm^{3+} microspheres is higher than that of the Y_2O_3:Yb^{3+}/Tm^{3+} microspheres. It may attribute to the well-crystallized structures and different bond energy between F-O and metal-O.

3.3. UC Mechanisms

Fig. 5 shows the energy level of the involved Tm^{3+} and Yb^{3+} ions as well as the proposed upconversion pathways under laser excitation with 980 nm. According to the energy level diagrams of Tm^{3+} and Yb^{3+} ions, blue, green and red upconversion emission were observed, and the commonly acceptable mechanisms can be expressed as shown in Fig. 5. One energy transfer step from the Yb^{3+} ion to the Tm^{3+} ion populates the $^3H_5$ level of Tm^{3+} from the $^3H_6$ state. The $^3H_5$ state relaxes nonradiatively to a lower $^3F_4$ state. The second energy transfer step raises the Tm^{3+} ion from $^3F_4$ state to $^3F_{2,3}$ state and then relaxes by the multi-phonon assisted process to the $^3H_4$ state. Subsequently, the third transfer raises the $^3H_4$ state to the $^1G_4$ state. The way to populate the $^1D_2$ state is through cross relaxation between adjacent Tm^{3+} from the $^3F_2$ state to the $^3H_6$ state and the $^3H_4$ state to the $^1D_2$ state. The strong blue emission at 477 nm corresponds to transitions from the $^1G_4$ to $^3H_6$ state of Tm^{3+}. The radiative decay from $^1D_2$ state to the $^3H_5$ state of the Tm^{3+}

generates an emission at 540 nm. The red emission at 647 and 692 nm corresponds to the $^1G_4$ state to $^3F_4$ state and the $^3F_3$ state to the $^3H_6$ state transition of the Tm^{3+} [31,34].

To understand UC mechanisms of energy transfer, the pumping power dependence of UC emission intensity (I_{UC}) was measured. In unsaturated UC process, the number (n) of photons absorbed per upconverted emitting state can be described as the relation $I_{UC} \propto P^n$, where P is the power of excitation source and n is the number of photons which can be readily determined from the slope of I_{UC}-P plot in a log-log scale [35]. As shown in Fig. 6a, the value(n) at 647- and 692 nm are 1.52, 1.53, respectively, indicating a two-photon UC process. Then n≈1 is observed for 477-, and 540- nm three-photon UC radiations. It(n) is less than the expected photon numbers absorbed for the corresponding emission. This proves that saturation process has occurred for generation of the UC [36-39]. In upconversion mechanism, attribute to the competition between linear decay and upconversion processes for the depletion of the intermediate exited states, the dependence of UC intensity on pump power is expected to decrease in slope. This phenomenon was theoretically described by Pollnau *et al* to the "saturation" process [40]. To confirm the proposed upconversion paths, the lower pump power was used to measure the pumping power dependence of UC emission intensity (I_{UC}) in Fig. 6b. Slope values of the linear are 2.56, 1.85, 2.86 for the UC bands at 477, 692 and 647 nm. The results indicate that three photons are necessary to produce the UC emission center at 477 and 647 nm and two photons to produce the emission center at 692 nm, which fits with the proposed upconversion pathways.

4. Conclusions

$Y_7O_6F_9$ microparticles codoped with Yb^{3+}-Tm^{3+} ions were prepared by an ionic liquid-assisted hydrothermal process. Efficient UC emission spectrum can be observed in the microspheres under

excitation at 980 nm. Due to highly crystalline structures and lower phonon energy of oxyfluorides, the UC emission of $Y_7O_6F_9$ samples has higher intensity under weak excitation power (10 mW) than Y_2O_3 samples. The IL is used not only as the reaction medium to influence the samples morphology and crystallization property, but also as the source of F^-. These results show a new way for enhancing UC emission in rare-earth ions doped $Y_7O_6F_9$ materials by ionic liquid-assisted hydrothermal process. This work will evoke wide interest in color displays, multicolor fluorescent labels, and photonic applications of these microcrystals.

References

1 Z. He, X.Y. Sun, X. Gu, Ceram. Int. 43(2017)7378-7382.
2 T. Pang, W. H. Lu, Ceram. Int. 43(2017) 1061-1065.
3 K. Binnemans, Chem. Rev. 109(2009) 4283-4374.
4 S. Ivanova, F. Pellé, A. Tkachuk, M. F. Joubert , Y. Guyo, V.P. Gapontzev, J. Lumin. 128(2008) 914-917.
5 R. Cai, H. Lian, Z. Hou, C. Zhang, C. Peng, J. Lin, J. Phys. Chem. C. 114(2010) 610-616.
6 J. Zhou, Z. Liu, F. Li, Chem. Soc. Rev. 41(2012) 1323-1349.
7 F. Wang, D. Banerjee, Y. S. Liu, X. Y. Chen, X. G. Liu, Analyst 135(2010) 1839 -1854.
8 X. Y. Huang, S. Y. Han, W. Huang, X. G. Liu, Chem. Soc. Rev. 42(2013)173-201.
9 X.Ye, J. E. Collins, Y.Kang, J.Chen, D.Chen, A.Yodh, C.Murray, Proc. Natl. Acad. Sci. U. S. A. 107 (2010) 22430-22435.
10 M.M. Xu, Z.J. Zhang, J.T. Zhao, J.Z. Zhang, Z.W. Liu, J. Alloy. Compd. 647(2015) 1075 - 1080.
11 K.Z. Zheng, W.P. Qin, C.Y. Cao, D. Zhao, L.L. Wang, J. Phys. Chem. Lett. 6(2015) 556 - 560.
12 Z.G. Xia, A. Meijerink, Chem. Soc. Rev. 46(2017) 275-299.
13 J. L. Wu, B. S. Cao, F. Lin, J. Chen, J. S. Sun, B. Dong, Ceram. Int. 42(2016) 18666-18673.
14 F. Auzel, Phys. Rev. B 13(1976) 2809-2817.
15 F. Wang, R. Deng, J. Wang, Q. Wang, Y. Han, H. Zhu, X. Chen, X. Liu, Nature Mater. 10 (2011) 968-973.
16 D. T Klier, M.U. Kumke, J. Phys. Chem. C. 119 (2015) 3363-3373.
17 C. A. Traina, J. Schwartz, Langmuir 23(2007) 9158-9161.
18 Y.H. Zhang, S.B. Li, F. Qin, Z.G. Zhang, Z.W. Dai, J. Opt. Soc. Am. B. 32(2015) 1856-1860.
19 G. Chen, Y. Liu, Y. Zhang, G. Somesfalean, Z. Zhang, Q. Sun, F. Wang, Appl. Phys. Lett. 91 (2007) 133103.
20 M. Ma, C.F. Xu, L.W. Yang, G.Z. Ren, J.G. Lin, Q.B.Yang, Physica. B 406(2011) 3256 - 3260.
21 L. Tao, W. Xu, Y. S. Zhu, L. Xu, H. C. Zhu, Y.X. Liu, S. Xu, P.W. Zhou, H.W. Song, J. Mater. Chem. C. 2 (2014) 4186-4195.
22 S. Park, W. Yang, C.Y. Park, M. Noh, Seulki, Choi, D, Park, H.S. Jang, S.H. Cho, Mater. Res. Bull. 71(2015) 25-29.
23 C.Y. Park, S. Park, J. Lumin. 178(2016) 463-469.
24 W. Yang, S.H. Kim, S.G. Park, J. Alloy. Compd. 673(2016) 1-7.
25 W. Yang, S. Park, Rsc. Adv. 6 (2016) 12652-12656.
26 F. Wang, D. Banerjee, Y.S. Liu, X.Y. Chen, X.G. Liu, Analyst 135(2010) 1839-1854.
27 J. Dupont, C.S. Consorti, P.A.Z. Suarez, R.F.D. Souza, Org. Synth. 79(2003) 236-243.
28 L.B. Zong, P.F. Xu, Y.J. Ding, K. Zhao, Z.M. Wang, X.C. Yan, R. B.Yu, Small 11(2015) 2768-2773.
29 J.B. Zhao, L.L. Wu, K. Zou, Mater. Res. Bull. 46 (2011) 2427-2432.
30 W.J. Zheng, X.D. Liu, Z.Y. Yan, ACS Nano. 3(2009) 115-122.
31 W.J. Huang, M.Y. Ding, H.M. Huang, C.F. Jiang, Y. Song, Y. R. Ni, C. H. Lu, Mater. Res. Bull. 48(2013) 300-304.
32 P. Amitava, Chem. Phys. Lett. 387(2004) 35-39.
33 J.B. Zhao, L.L. Wu, C.J. Zhang, B.Zeng, J. Mater. Chem. C 5(2017) 3903-3907.
34 J.P. Jouart, M. Bouffard, T. Duvaut, N.M. Khaidukov, Chem. Phys. Lett. 366(2002) 62–66.

35 Y.H. Zhang, S.B. Li, F.Qin, Z.G. Zhang, Z.W. Dai, J. Opt. Soc. Am. B 32(2015) 1856-1860.
36 G.Y. Chen, H.J. liang, H.C. Liu, G. Somesfalean, Z.G. Zhang, Opt Express 17 (2009) 16366-16371.
37 A. Pandey, V. K. Rai, R. Dey, K. Kumar, Mater. Chem. Phys. 136(2013)483-488.
38 M. Mondal, V. K. Rai, C. Srivastava, Chem. Eng. J. 327(2017)838-848.
39 M. Mondal, V. K. RAi, C. Srivastava, S. Sarkar, R. Akash, J. Appl. Phys. 120(2016)233101.
40 M. Pollnau, D R. Gamelin, S.R. Luthi, H.U. Güdel, Phys. Rev.B 61(2000) 3337-3346.

Figures and Figure Caption:

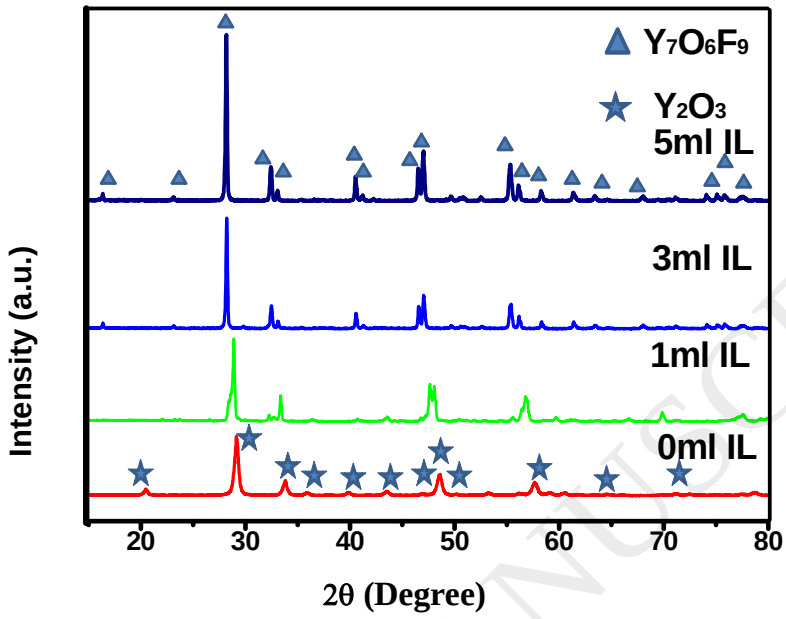

Fig. 1 XRD patterns of prepared products with different IL concentrations.

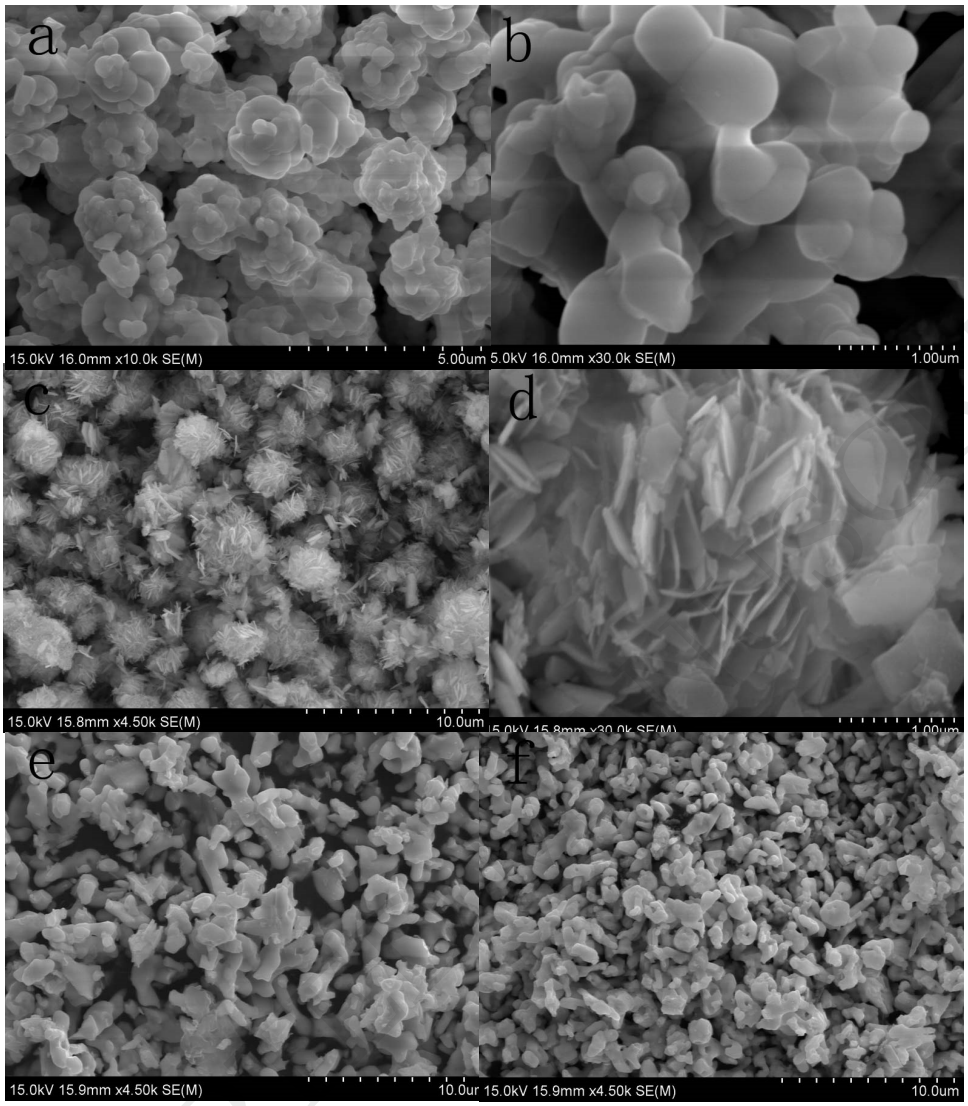

Fig. 2 FE-SEM images of the samples: **(a)** and **(b)** $Y_7O_6F_9$:Yb^{3+}/Tm^{3+} sample prepared with 5 mL IL; **(c)** and **(d)** Y_2O_3:Yb^{3+}/Tm^{3+} sample prepared without IL; **(e)** nanoparticles prepared with 1 mL IL; and **(f)** $Y_7O_6F_9$:Yb^{3+}/Tm^{3+} sample prepared with 3 mL IL.

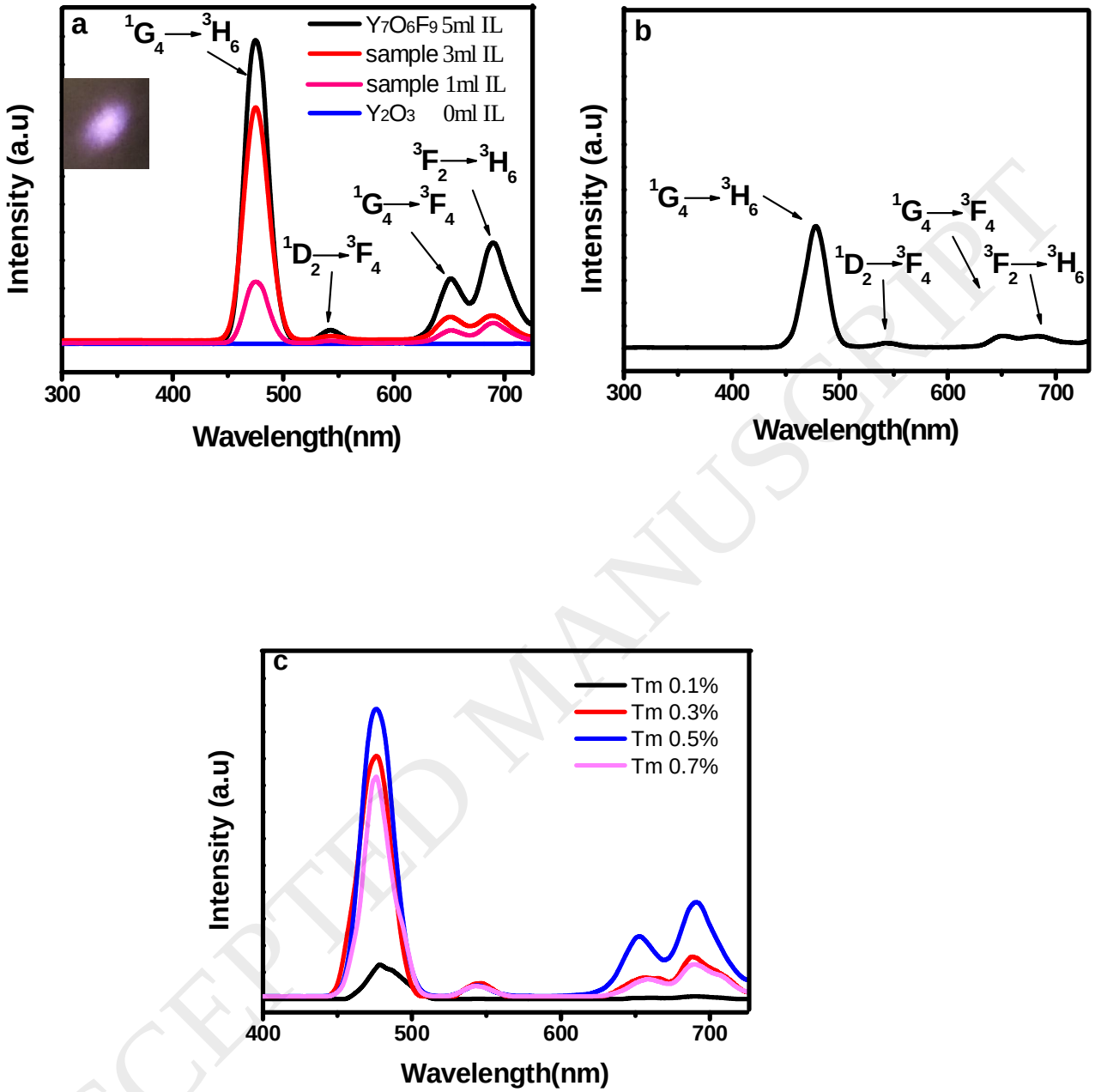

Fig. 3 (a) Upconversion emission spectra of samples with different concentration of IL excited by 980 nm unfocused laser beam with a pump power of 10 mW. The inset is the photographic image of upconversion photoluminescence $Y_7O_6F_9$:Yb^{3+},Tm^{3+} (5 mL IL) microsphere under the unfocused laser excitation at 980 nm of 10 mW (pump power density of only ~0.1 W/cm^2); **(b)** upconversion emission spectra of Y_2O_3: Yb^{3+}, Tm^{3+} excited by 980 nm unfocused laser beam with a pump power 1000 mW; and **(c)** upconversion emission spectra

with different concentration of Tm^{3+} doped $Y_7O_6F_9$:Yb^{3+},Tm^{3+} (5 mL IL) microsphere under 980 nm laser excitation.

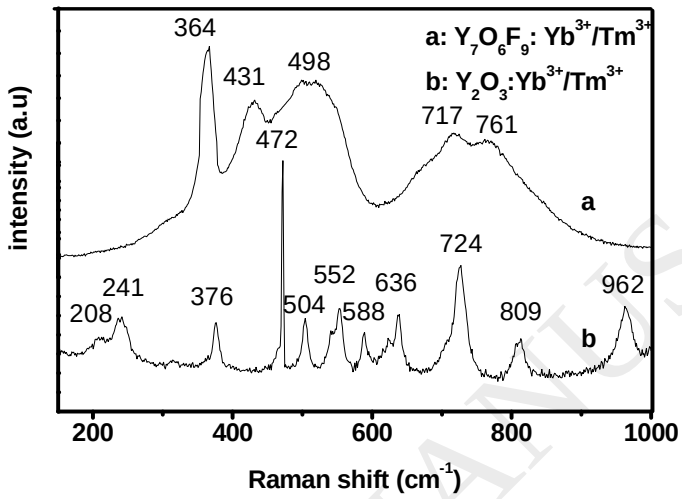

Fig. 4 Raman spectra of (a) $Y_7O_6F_9$:Yb^{3+},Tm^{3+}, (b) Y_2O_3: Yb^{3+}, Tm^{3+} with the same doping condition at room temperature.

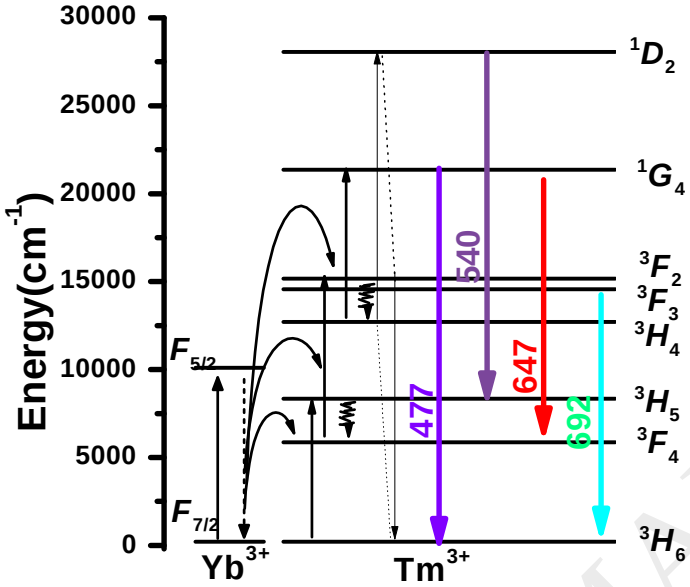

Fig. 5 Diagram of the energy levels of the Tm^{3+} and Yb^{3+} ions and the proposed mechanisms of upconversion.

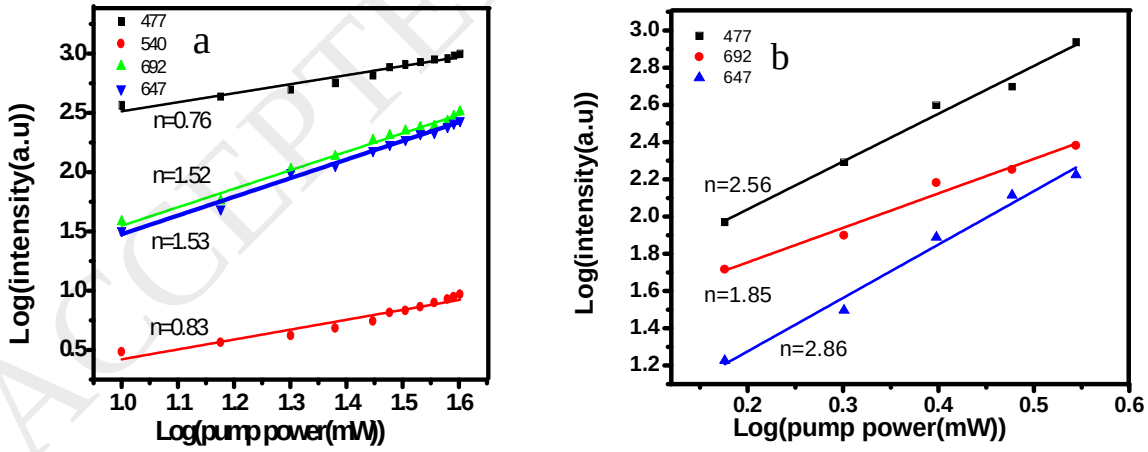

Fig. 6 Pump power dependence of the emission intensity of different transitions in the $Y_7O_6F_9$:Yb^{3+},Tm^{3+}

microspheres (a) saturated UC process (the pump power is higher than 10 mW), (b) unsaturated UC process (the pump power is lower than 3.5 mW).